PNAS RESEARCH ARTICLE | CHEMISTRY OPEN ACCESS

Dependence on relative humidity in the formation of reactive oxygen species in water droplets

Mohammad Mofidfar[a], Masoud A. Mehrgardi[a,b], Yu Xia[a], and Richard N. Zare[a,1]

Contributed by Richard N. Zare; received September 13, 2023; accepted February 8, 2024; reviewed by Agustín J. Colussi, Bengt Nordén, and Zhong L. Wang

Water microdroplets (7 to 11 μm average diameter, depending on flow rate) are sprayed in a closed chamber at ambient temperature, whose relative humidity (RH) is controlled. The resulting concentration of ROS (reactive oxygen species) formed in the microdroplets, measured by the amount of hydrogen peroxide (H_2O_2), is determined by nuclear magnetic resonance (NMR) and by spectrofluorimetric assays after the droplets are collected. The results are found to agree closely with one another. In addition, hydrated hydroxyl radical cations ($•OH\text{-}H_3O^+$) are recorded from the droplets using mass spectrometry and superoxide radical anions ($•O_2^-$) and hydroxyl radicals (•OH) by electron paramagnetic resonance spectroscopy. As the RH varies from 15 to 95%, the concentration of H_2O_2 shows a marked rise by a factor of about 3.5 in going from 15 to 50%, then levels off. By replacing the H_2O of the sprayed water with deuterium oxide (D_2O) but keeping the gas surrounding droplets with H_2O, mass spectrometric analysis of the hydrated hydroxyl radical cations demonstrates that the water in the air plays a dominant role in producing H_2O_2 and other ROS, which accounts for the variation with RH. As RH increases, the droplet evaporation rate decreases. These two facts help us understand why viruses in droplets both survive better at low RH values, as found in indoor air in the wintertime, and are disinfected more effectively at higher RH values, as found in indoor air in the summertime, thus explaining the recognized seasonality of airborne viral infections.

viral infection seasonality | relative humidity | microdroplets | hydrogen peroxide | reactive oxygen species

Significance

Relative humidity (RH) plays a crucial role in virus viabilities in respiratory droplets that leads to seasonality patterns in the spread of airborne viral infections; but its mechanism has not been established. Perhaps, the solution to this puzzle lies in part in the formation of reactive oxygen species (ROS) as disinfectants within microdroplets, intricately tied to its reliance on RH. Notably, we find a strong correlation between ROS concentration trends in water microdroplets at different RH levels and reported virus viability trends. The robust alignment of these trends highlights the pivotal role of ROS as a disinfectant factor, influenced by RH. This understanding suggests changes in strategy for reducing the spread of such infections.

The airborne transmission of respiratory viruses significantly affects health, morbidity, mortality, and economic losses, as evident from the ongoing COVID-19 pandemic (1). As of February 2023, the Center for Systems Science and Engineering at Johns Hopkins University has reported more than 675 million cases and more than 6.8 million deaths around the world attributable to COVID-19 (2). Respiratory droplets emitted while coughing, sneezing, breathing, and speaking span diverse sizes. The size depends on the generation mechanism and the site of origin, influenced by the shear force generated by airflow within the respiratory tract (3). Long-distance transmission occurs through the evaporation of droplets, enabling infection between individuals who have not had face-to-face contact or shared the same room (4). Bax and coworkers from the NIH have carefully examined solid evidence supporting airborne transmission via speech as the primary route for the transmission of SARS-CoV-2 (5). Emerging evidence highlights a significant correlation between the indoor relative humidity (iRH) of air and viral respiratory infections (6–10), with a heightened risk of viral respiratory illnesses strongly linked to lower RH levels below 40%. Investigations in animal models have also demonstrated that RH can influence the airborne transmission of influenza A viruses, leading to reduced transmission rates at high and intermediate RH levels (11, 12).

Analysis of the dynamics of influenza and COVID-19 across seasons clearly shows that the quantity of virus shed is significantly higher during winter and rarer in the summertime. Considering that people in temperate regions spend more than 80% of their time indoors, regardless of external weather conditions (10, 13–15), it is reasonable to anticipate that the majority of respiratory infections would occur in these indoor settings (16), where iRH levels can easily drop below 40% (8, 10, 17–22). Climate data for COVID-19 transmission were collected from the outdoor environment to inform spreading distancing guideline and prevent COVID-19 transmission. In contrast, some studies have explored the impact of heating, ventilation, and air conditioning systems on the spread of respiratory viruses (23, 24). Accumulating evidence suggests that this seasonal variation is closely linked to iRH (7, 25, 26). These facts indicate the importance of being mindful about increasing iRH levels in the indoor spaces we occupy 80 to 90% of the time, whether in summertime or wintertime.

Author affiliations: [a]Department of Chemistry, Stanford University, Stanford, CA 94305; and [b]Department of Chemistry, University of Isfahan, Isfahan 81743, Iran

Author contributions: M.M. and R.N.Z. conceptualized and designed research; M.M. and M.A.M. equally contributed to performing experiments and analyzing data; and Y.X. carried out EPR experiments. All authors contributed to writing and editing the paper.

Reviewers: A.J.C., California Institute of Technology; B.N., Chalmers tekniska hogskola; and Z.L.W., Georgia Institute of Technology.

The authors declare no competing interest.

[1]To whom correspondence may be addressed. Email: zare@stanford.edu.

This article contains supporting information online at https://www.pnas.org/lookup/suppl/doi:10.1073/pnas.2315940121/-/DCSupplemental.

Published March 15, 2024.

Temperate-zone winters often lead to an increase in the spread of respiratory viruses (7, 27). Recent studies have attempted to link temperature and humidity to the seasonal pattern of COVID-19 infection rates (10, 22, 28–30). Heating a building typically dries the air and decreases iRH, which improves the virus's viability and weakens immune defenses (25). Many studies have shown qualitative patterns in the survivability of virus at high temperatures and a U-shaped effect of RH in droplets and aerosols (31, 32). Numerous reasons for these findings have been proposed, including theories about the virus-killing powers of sunlight, extra immune-boosting doses of vitamin D in summer, the disease-spreading influence of schools during wintertime, and the effect of droplet pH and surrounding CO_2 (6, 7, 33–35). While various articles have reported the influence of humidity on the transmission of respiratory droplets, most of them focused on experimental and theoretical models of the impact of humidity on evaporation rates, which ultimately affect droplet size, settling time, and the distance these droplets can travel before eventually settling (36–40).

Respiratory droplets exhibit a wide size range, spanning from submicrometers to thousands of micrometers (37, 38, 41, 42). Droplets larger than 200 μm settle to the ground in less than 1 s (36). Studies conducted by Marr et al. (37) in 2018 and Dhawan et al. (36) in 2021 analyzed the settling time of a protein-containing droplet initially 10 μm in diameter under various RH levels. The results indicated that decreasing RH from 100 to 90% and below 64% led to a reduction in droplet size, from 10 μm to 2.8 μm and 1.9 μm, respectively. Additionally, the lifetimes for these droplets were calculated to be 8 min, 102 min, and 216 min, respectively.

While evaporation rates at different RH levels and their impact on droplet size, settling time, and travel distance are crucial, these are not the only factors governing the seasonal pattern of viral infections. A previous study also reported a similar trend demonstrating an increase in the bactericidal effect of microdroplets as RH increases but lacked a systematic investigation (9). This study delves into the intricate puzzle of virus instability within droplets, proposing a connection to the formation of reactive oxygen species (ROS) at the surface of microdroplets at different RH levels. These ROS have the potential to act as disinfectant agents, rendering viruses ineffective within exhaled droplets. Here, we present experimental proof of the impact of humidity levels on ROS concentration as measured primarily by hydrogen peroxide (H_2O_2) formation in nebulized H_2O and D_2O droplets. Moreover, we suggest a mechanism based on electron transfer at the water microdroplet interface aided by the strong electric field present and the partial solvation of ions.

Results

Mass Spectrometric Analysis of Microdroplets. Nebulized H_2O and D_2O underwent mass spectrometric analyses, and the resulting ion currents versus RH for different *m/z* values are depicted in Fig. 1. For water microdroplets, a discernible peak at *m/z* = 36, corresponding to $\bullet OH\text{-}H_3O^+$, is observed. This result indicates that the ion current rises with higher RH levels, highlighting the importance of water molecules' interaction at the air–water interface in H_2O_2 formation. Previous work also reported the same trend but lacked a systematic study (43). In contrast, when D_2O is employed instead of H_2O while maintaining H_2O in the air surrounding the microdroplet, five peaks appear at *m/z* = 36, 37, 38, 39, and 40, corresponding to different amounts of D exchanging for H. The ion currents for *m/z* = 36 at RH > 15% were nearly zero but gained intensity with increasing humidity, although they remained relatively inferior to the ion currents of other *m/z* values. On the other hand, the ion current for *m/z* = 40 ($\bullet OD\text{-}D_3O^+$) is maximum at low humidity and remained relatively constant up to 50% humidity, decreasing with further increases in RH and reaching negligible values at RH > 75%. Furthermore, the ion currents for *m/z* = 37, 38, and 39 exhibit high intensities compared with the ion currents for *m/z* = 36 at low humidity. They progressively increase up to 50% RH and then gradually decline as the RH level grows. These observations lead us to conclude that individual water molecules in the surrounding atmosphere of microdroplets can form a partial layer as separated islands on the surface of microdroplets, which gradually grow with increasing RH. Eventually, at RH > 75%, the water islands merge to form a complete layer around the droplets. Therefore, at RH > 75%, $\bullet OD\text{-}D_3O^+$ (*m/z* = 40) disappears, and $\bullet OD\text{-}H_3O^+$ reaches its maximum value and remains almost constant. The diffusion of D_2O molecules inside this layer and H-to-D exchange cause peaks to emerge at *m/z* = 37, 38, and 39.

The data demonstrate that the presence of water molecules in the air bombarding the H_2O or D_2O droplet interface facilitates the process, accounting for the increase in H_2O_2 with higher RH.

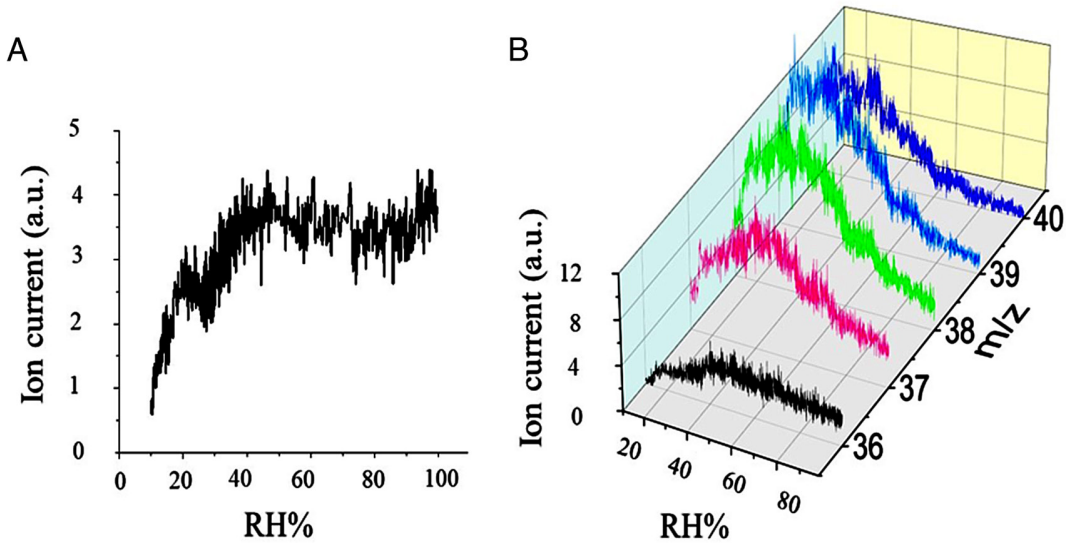

Fig. 1. The $\bullet OH\text{-}H_3O^+$ signal in the mass spectrum of sprayed water (*A*) and the hydrated hydroxyl radical cation from D_2O microdroplets (*B*) surrounded by air containing H_2O at different RH levels.

This behavior is in agreement with earlier work by Wilson and coworkers who pointed out the importance of gas-phase reactions in water microdroplets (44). Additional evidence supporting the acceleration of reactions in the surface region and the attainment of exceptionally high-rate constants can be observed in the ion current for *m/z* = 36 (corresponding to •OH-H_3O^+), notably lower than those of the other ion currents. This phenomenon indicates that the overall acceleration of droplet reactions surpasses the contribution attributed solely to the surface fraction. Within the droplet, reactants access the air–water interface, undergo reactions, and subsequently diffuse into the droplet bulk. In the case of *m/z* = 36, no H_2O molecules are available in the D_2O droplet to diffuse to the surface and only originated from the water molecules in the surrounding air, leading to a much lower ion current. Conversely, for *m/z* = 37, 38, 39, and 40, the reactant (D_2O) can efficiently diffuse from the bulk to the surface, contributing to higher ion currents in these cases.

This highlights the significance of reactions at the air–water interface in enhancing reaction rates and ion currents within microdroplets.

These observations have led to the following proposed mechanism for H_2O_2 formation in microdroplets, in agreement with the work of Colussi (45):

$$(H_2O)_2 \rightarrow H_3O^+ + OH^-. \quad [1]$$

At the interface, OH^- and H_3O^+ cluster together, creating a strong electric field that drives electron loss from OH^- (forming •OH) and $(H_2O)_2$ (forming •OH-H_3O^+).

This phenomenon accounts for the measurable current observed at the solid interface and explains the formation of O_2^- when O_2 molecules strike the air–water interface.

Specifically at the interface, not within the bulk or interior of the droplet, the following reaction takes place:

$$OH^- + H_3O^+ \rightarrow \cdot OH + \cdot H + H_2O. \quad [2]$$

The partial solvation of H^+ and OH^- aids in this reaction. The hydrogen radical (•H) can subsequently hydrogenate other species at the interface, such as N_2 adsorbed on a metal oxide surface (46), or it can recombine with itself:

$$\cdot H + \cdot H \rightarrow H_2. \quad [3]$$

The presence of an overwhelming amount of water makes the H atom more likely to react with water itself:

$$\cdot H + H_2O \rightarrow H_2 + \cdot OH. \quad [4]$$

The hydroxyl radicals can combine to form H_2O_2:

$$\cdot OH + \cdot OH \rightarrow HOOH. \quad [5]$$

By combining Eqs. **1**–4, we obtain the following overall reaction:

$$(H_2O)_2 \rightarrow HOOH + H_2. \quad [6]$$

Quantification of H_2O_2 Formation Using NMR. The effect of humidity on the concentration of H_2O_2 in microdroplets was investigated using NMR. As Fig. 2 illustrates, when chamber RH increases from 15 to 50%, the concentration of H_2O_2 increases from 0.6 μM to 2.0 μM. By investigating higher RH levels, specifically in the range of 50 to 95%, we found that varying the humidity led to a lowered H_2O_2 concentration (1.4 μM). It is worth noting that we should consider the diluted concentration and evaporation rate during the collection of water microdroplets in the chambers. At low RH, droplet evaporation is much higher than at high RH (43). This means that at high RH, water microdroplets are more diluted than at lower RH levels. Based on our findings illustrated in Fig. 2, we observed a correlation between the concentration of H_2O_2 and the RH of the sprayed water microdroplets. These observations demonstrate the strong influence of RH on the formation of H_2O_2. Additionally, when the humidity increased to levels between 50 and 95%, we observed a slight decrease in H_2O_2 concentration, supporting the U-shaped virus viability behavior reported previously. The findings of this study lay the groundwork for further investigations into the influence of humidity on the seasonality of airborne viral infections.

Effect of Droplet Size and Flow Rate on the Formation of ROS. To investigate the role of particle size in the formation of H_2O_2, we conducted a study employing various flow rates to generate microdroplets with different sizes (*SI Appendix*, Fig. S1). As shown in Fig. 3*A*, a decrease in the flow rate of nebulized water microdroplets from 150 to 60 μL/min results in a reduction in the average droplet size from 11.1 to 7.3 μm. The impact of microdroplet size on H_2O_2 formation was a key focus of our investigation. In addition, we observed that as the diameter of the

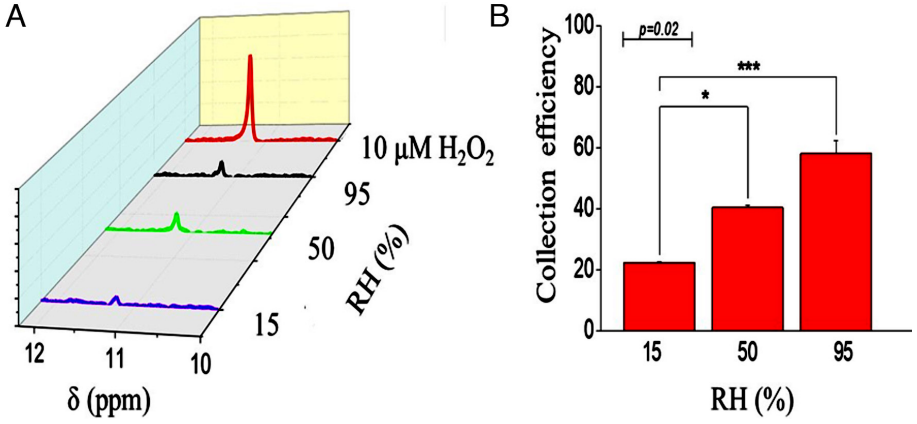

Fig. 2. NMR results of sprayed water microdroplets and collection efficiency for the formation of H_2O_2 at different values of the humidity (*A*), and the collection efficiency of microdroplet formation (*B*) at three different humidities (15%, 50%, and 95%). The red spectrum represents 10 μM H_2O_2, used as a control, whereas the black, green, and pink spectra represent water microdroplets at an injection rate of 60 μL/min that were humidified at 15%, 50%, and 95% RH, respectively.

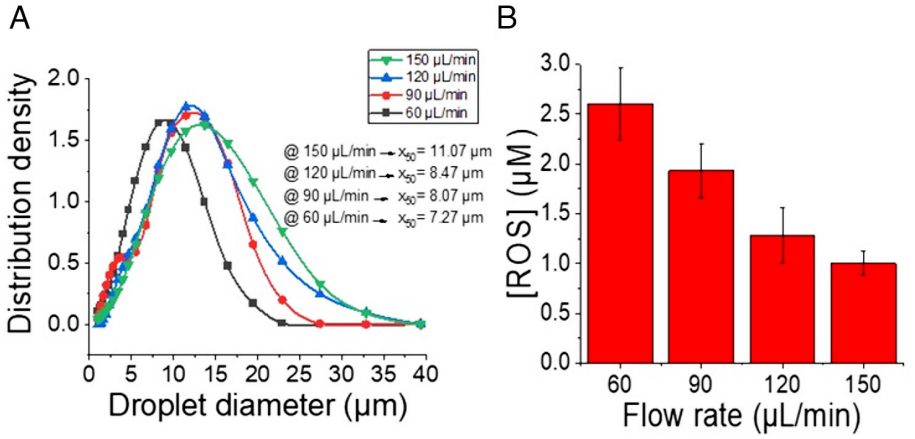

Fig. 3. The dependence of droplet distribution density with droplet diameter at different flow rates (60, 90, 120, and 150 µL/min) at constant air pressure (90 psi) with 50% ± 4% RH (*A*), and ROS concentration dependence to the flow rate of compressed air at a constant volume collection of 200 µL (*B*).

microdroplets decreased to about 10 µm or less, the yield of H_2O_2 increased. This finding indicates that microdroplet diameters have an important effect on the formation of H_2O_2, which has been reported previously (47, 48). Based on our observations in Fig. 3*B*, the concentration of H_2O_2 is linked to the water flow rate controlled by a syringe pump. This relationship could potentially influence the distribution of microdroplet sizes. While nebulizing, as water microdroplets undergo evaporation, H_2O_2 concentration increases due to the higher boiling point of H_2O_2 compared with water. This phenomenon could explain the observed link between H_2O_2 concentration and flow rate. To determine how H_2O_2 concentration in water microdroplets responds to droplet sizes, we measured droplet size distribution density and average droplet sizes at different flow rates. By carefully analyzing these data points, we were able to discern patterns and gain deeper insights into the relationship between droplet size and H_2O_2 concentration. As the flow rate of water decreases, the surface-to-volume ratios of the microdroplets increase.

Qualitative Analysis of Free Radicals in Sprayed Water Microdroplets. Electron paramagnetic resonance spectroscopy (EPR) spectroscopy is utilized for the qualitative analysis of free radicals in water microdroplets sprayed under different atmospheres, including hydroxyl radicals (•OH), superoxide radical anions ($\bullet O_2^-$), and hydrogen radicals (•H). As depicted in Fig. 4*A*, under a nitrogen (inert) atmosphere, clear signals for both hydrogen and hydroxyl radicals can be observed in water microdroplets. In contrast, water microdroplets in an air atmosphere only display signals for hydroxyl radicals. This observation can be attributed to the potent reductive nature of hydrogen radicals in the water microdroplets, which rapidly react with oxidative species in the environment, such as oxygen. The results for superoxide radical anions further support this conclusion. In Fig. 4*B*, water microdroplets in the inert atmosphere show negligible signals for superoxide radical anions, whereas those in air reveal a prominent superoxide radical anion signal. This confirms that oxygen can react with reductive radicals to produce superoxide radical anions, suggesting an important contribution to forming H_2O_2 in the water microdroplets, as previously observed (47).

Discussion

Many viral infections are spread by exhaled droplets from the breath of sick individuals. Numerous studies have reported a seasonal variation in the incidence of disease, which peaks as the air becomes drier in the winter versus the summer, caused by the heating of indoor air to keep occupants warm. In this study, we propose an explanation for this behavior based on measuring the concentration of the disinfectant H_2O_2 in water droplets as a function of the RH of air surrounding the droplets. The

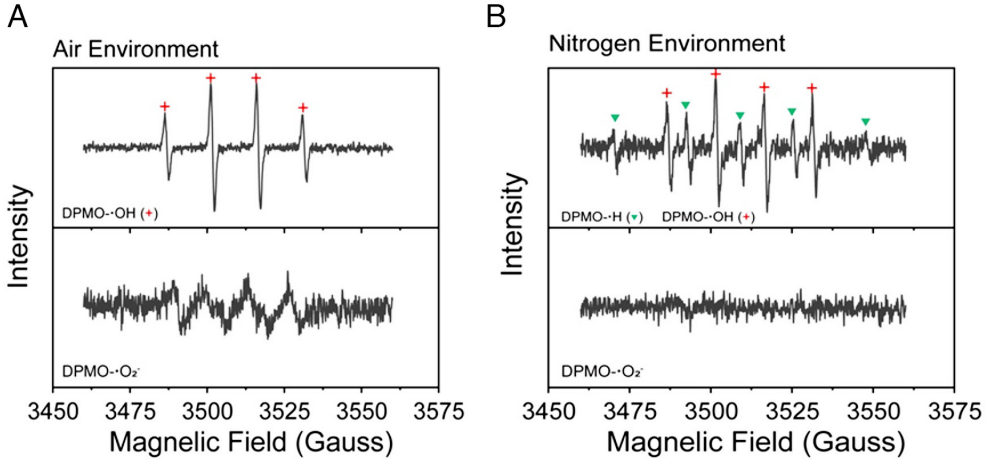

Fig. 4. ESR spectrum of sprayed water microdroplets for the detection of hydroxyl radicals (•OH), superoxide radical anions ($\bullet O_2^-$), and hydrogen radicals (•H) by 5 mM solution of DMPO sprayed in (*A*) air and (*B*) nitrogen.

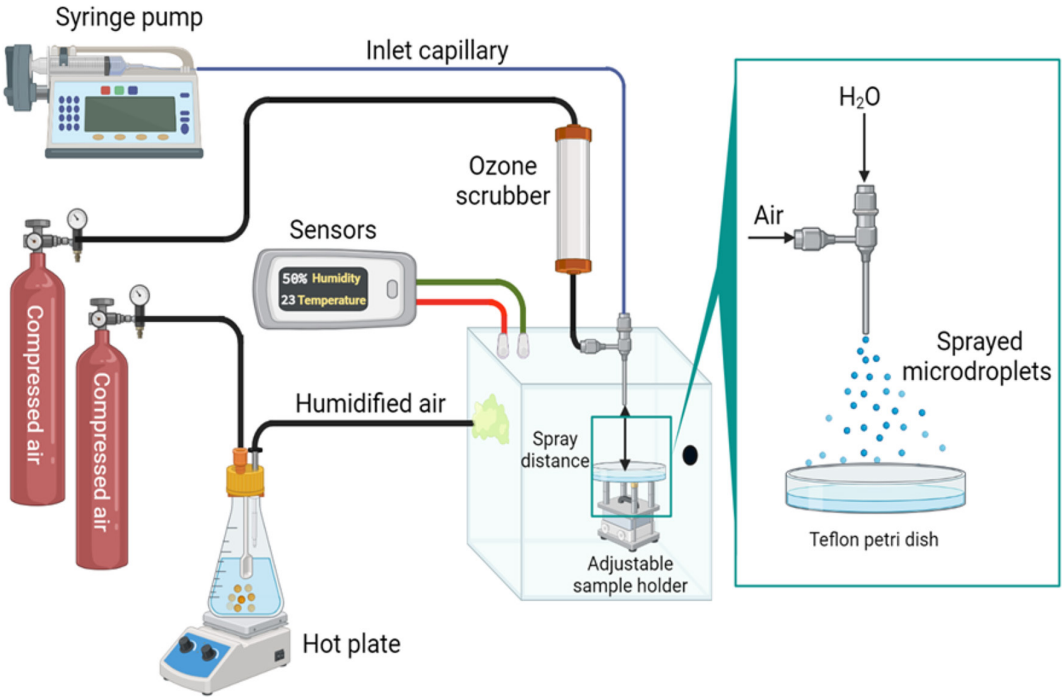

Fig. 5. Diagram illustrating the experimental setup for the generation and collection of aqueous microdroplets.

concentration of H_2O_2 and related ROS at various RH levels was obtained via mass spectrometric, NMR, and spectrofluorimetric techniques. The findings reveal that as the RH increases, the ROS concentration also grows. When this fact is combined with the accelerated rate of droplet evaporation as the RH decreases, and thus the shorter time that viruses in droplets interact with ROS, we gain an understanding of the importance of RH in controlling the spread of airborne viral infections.

During the winter, iRH levels in both residential apartments and commercial buildings drop to less than 24%, while maintaining a comfortable temperature range of 20 to 24 °C (49, 50). When small droplets are expelled into the dry air, they rapidly evaporate, and the viruses can stay suspended in the air for long periods of time. In contrast, larger droplets have a shorter travel distance before falling to the ground. Evaporation prevails over condensation when a water microdroplet is surrounded by air not saturated in water vapor. Evaporation, however, is a complex process controlled primarily by air temperature and RH involving the interplay of combined mass and heat transfer occurring in the droplet. This phenomenon has been carefully modeled by Netz (51). Not surprisingly, the rate of shrinkage of the water microdroplet depends sensitively on RH for a given air temperature. For example, for droplets with radii ranging from 70 nm to 60 μm, evaporation follows the stagnant-flow approximation. In an enclosed space of midsize, an infected person speaking without a mask constantly emits over 10^4 viruses into the air, resulting to a minimum viral inhalation rate of 2.5 per minute.

The effect of RH and temperature on the stability of respiratory viruses has also been extensively studied, and the viral surface proteins and lipid membranes suspended within droplets are closely linked to droplet evaporation and the resulting supersaturation of the enclosed ingredients (52–56). Studies using guinea pigs and ferrets as animal models have shown that high RH (>60%) and low RH (<40%) favor the viability of influenza viruses in droplets, whereas intermediate RH (40 to 60%) leads to viral inactivation (11, 12, 57). Marr and coworkers reported that air sampled near a patient contained an average of 60% more viral loads in comparison to samples collected at a distance greater than 1.8 m (58). These authors described this behavior as a mystery how could an increase in RH surrounding a respiratory droplet affect viruses that are not exposed to ambient air and therefore would not directly interact with water vapor in the air (37).

The mechanism behind the dependence of virus stability in microdroplets on surrounding humidity was unknown until now, although it was assumed that temperature and humidity affect viral surface proteins and lipid membranes (11, 12, 52, 57, 59). In this study, we propose an explanation for the formation of ROS at the air–water interface of microdroplets at different RH levels. The presence of water molecules in the air colliding with water at the droplet interface facilitates a process that leads to an increase in ROS as a function of higher RH. ROS, being a potent disinfection agent, has the potential to render viruses ineffective within exhaled droplets. This revelation provides a crucial insight into the role of humidity in modulating viral viability and may have implications for understanding viral transmission and controlling infectious diseases. These findings open up new avenues for research and may lead to the development of technologies to harness humidity as a tool in viral disinfection and public health protection.

Conclusion

The comprehensive analysis of microdroplets through mass spectrometry, NMR, and spectrofluorimetric techniques has unveiled a crucial link between RH and the formation of ROS at the air-water interface. These techniques, augmented by EPR, demonstrate ROS formation, the clustering of OH^- and H_3O^+ at the droplet interface, and the formation of the superoxide radical anion ($\bullet O_2^-$) when O_2 in the air contacts the water microdroplets, resulting in the generation of a strong electric field that drives electron loss from OH^- (forming $\bullet$OH), $(H_2O)_2$ (forming $\bullet$OH-H_3O^+), and $\bullet O_2^-$ forming the peroxide radical ($\bullet$OOH) and other ROS. This finding sheds light on the seasonal variation in the spread of viral infections and provides a compelling explanation

for the observed increase in disease incidence during the drier winter months. As RH levels rise, so does the concentration of ROS, including H_2O_2, within microdroplets. This phenomenon, combined with the accelerated rate of droplet evaporation in lower RH conditions, highlights the critical role of humidity in controlling the spread of airborne viral infections. In essence, this research opens new avenues for further investigation and the development of technologies to harness humidity as a means of controlling infectious diseases.

Materials and Methods

H_2O_2 (ACS reagent, 3 wt% and 30 wt% solutions in water) was purchased from Thermo-Fisher Scientific. Deuterium oxide and spectrofluorometric assay (MAK165) were ordered from Sigma-Aldrich (St. Louis, MO) and used as received. Teflon® FEP Petri Dish Liners (50 mm) were ordered from Fluorolab (Dover, NH). An ozone scrubber (model CDU-30) was purchased from Oxidation Technologies, LLC (Inwood, IA). In addition, 384-well clear bottom microplates (White, 120 μL) were purchased from Corning® (Corning, NY). RH and temperature were controlled using EZ Thermo-Hygrostat controller (Guangdong, China). A CLARIOstar (Ortenberg, Germany) microplate reader was used to determine H_2O_2 concentration in water microdroplets.

Experimental Setup. As Fig. 5 shows, a pneumatic nebulizer was employed with two coaxial capillaries, where the inside capillary contains water, and the outside capillary contains compressed air. The deionized water passed through a borosilicate capillary that had a 100 μm internal diameter and a 360 μm external diameter. The compressed air (100 psi) passes the external capillary through an ozone scrubber before nebulizing water. At different injection flow rates from 60 to 150 μL/min, water was sprayed on Teflon® FEP Petri Dish Liners, which were placed on an adjustable holder inside the chamber. The nebulizer nozzle was approximately 2 cm away from the base of the petri dish. Water microdroplets were collected on the Petri dish liner and were promptly transferred to Eppendorf or NMR tubes.

Microdroplet Size Measurements. We used a HELOS 2750 particle size analyzer (Sympatec, Clausthal-Zellerfeld, Germany) to measure the size of microdroplets generated from a coaxial nebulized spray device. To assess the distribution of droplet sizes, we employed an R3 lens capable of measuring particle sizes between 0.9 and 175 μm. The average droplet diameter was measured for each sample using PAQXOS 5.0.1 software (Sympatec GmbH) with the Fraunhofer theory and MIEE mode. The measurement was conducted four to ten times at a wavelength of 632.8 nm. To ensure no interference from the sheath gas affected the measurement, we baselined the instrument with the nitrogen flow active but without any liquid flow.

NMR Analyses. Quantification of H_2O_2 using NMR was performed based on the previously reported protocol by Kakeshpour and Bax with slight modifications (60). Briefly, 540 μL collected samples or H_2O_2 standard solution and 60 μL of 2-N-(morpholino) ethanesulfonic acid buffer solution (10 mM in D_2O, pH 6.00 ± 0.05) were transferred into 5 mm quartz NMR tubes. The NMR spectra were acquired using a Varian 600 MHz Inova NMR spectrometer equipped with a 5 mm hydrogen, carbon, nitrogen room-temperature probe. The data were collected at 2 °C using 1.5 ms Gaussian excitation centered at 11.1 ppm with a bandwidth of approximately 2 ppm at 600 MHz for 0.1 s acquisition time with a recycle delay 50 ms with 48,000 scans for a total time of approximately 140 min using a spectral width of 20,000 Hz.

Mass Spectrometric Analyses. Deionized water or D_2O with a flow rate of 20 μL/min is sprayed onto a chamber with controlled humidity while the nebulizer nozzle is placed in front of the mass spectrometer (MS) inlet with a distance at ~3.0 mm and inlet capillary temperature of the MS is adjusted to 150 °C. Radical ions were detected in scan mode ranging at *m/z* 20 to 40 under positive mode on the LTQ-XL MS (Thermo-Fisher, Waltham, MA).

Spectrofluorometric Analyses. Quantification of H_2O_2 concentration inside water microdroplets was accomplished by following the fluorometric hydrogen peroxide assay kit (FHPAK) protocol (Sigma-Aldrich, Catalog Number MAK165). MAK165 fluorimetric Sensitivity of 0.01 μM was reported for FHPAK. The standard H_2O_2 solutions and collected water microdroplets place up to 25 μL of the sample into the 384–well plates (white with clear bottom) and then the sample volume was adjusted to 25 μL using Assay Buffer. The fluorescence intensity at (λ_{ex} = 540/λ_{em} = 590 nm) was measured using a fluorescence BMG LABTECH's CLARIOstar multimode microplate reader.

Measurements of Free Radical Species. Hydroxyl radicals (•OH), superoxide radical anions ($\bullet O_2^-$), and hydrogen radicals (•H) were trapped by 5,5-dimethyl-1-pyrroline-N-oxide (DMPO) and detected by a A300 ESR spectrometer (Bruker) at ambient temperature. The two samples were collected in a nitrogen environment (glove box) and in an air environment. A 5 mM solution of DMPO was prepared in deionized water with dissolved oxygen removed. The DMPO solution was sprayed with nitrogen or air (30 μL/min, 120 psi) and collected in a quartz disk after high-temperature treatment (removal of surface groups). Finally, the samples were transferred to test tubes and sealed and then quickly frozen in liquid nitrogen to ensure that the free radicals could be consistently observed.

Data, Materials, and Software Availability. All study data are included in the article and/or *SI Appendix*.

ACKNOWLEDGMENTS. We thank Juan Li, Wuhan University, for help with the EPR experiments. We are also grateful to A. Bax, NIH for critical comments on an earlier draft. Support from the US Air Force Office of Scientific Research through the Multidisciplinary University Research Initiative program (FA9550-21-1-0170) is gratefully acknowledged.

1. N. H. Leung, Transmissibility and transmission of respiratory viruses. *Nat. Rev. Microbiol.* **19**, 528–545 (2021).
2. E. Dong, H. Du, L. Gardner, An interactive web-based dashboard to track COVID-19 in real time. *The Lancet Infect. Dis.* **20**, 533–534 (2020).
3. V. Stadnytskyi, P. Anfinrud, A. Bax, Breathing, speaking, coughing or sneezing: What drives transmission of SARS-CoV-2? *J. Inter. Med.* **290**, 1010–1027 (2021).
4. K. Mahjoub Mohammed Merghani, B. Sagot, E. Gehin, G. Da, C. Motzkus, A review on the applied techniques of exhaled airflow and droplets characterization. *Indoor Air* **31**, 7–25 (2021).
5. J. Andersson, What drives transmission of severe acute respiratory syndrome coronavirus 2? *J. Inter. Med.* **290**, 949–951 (2021).
6. C. C. Wang *et al.*, Airborne transmission of respiratory viruses. *Science* **373**, eabd9149 (2021).
7. A. Božič, M. Kanduč, Relative humidity in droplet and airborne transmission of disease. *J. Biol. Phys.* **47**, 1–29 (2021).
8. C. Verheyen, L. Bourouiba, Associations between indoor relative humidity and global COVID-19 outcomes. *J. R. Soc. Interface* **19**, 20210865 (2022).
9. M. T. Dulay *et al.*, Spraying small water droplets acts as a bacteriocide. *QRB Discov.* **1**, e3 (2020).
10. C. Guo *et al.*, Meteorological factors and COVID-19 incidence in 190 countries: An observational study. *Sci. Total Environ.* **757**, 143783 (2021).
11. A. C. Lowen, S. Mubareka, J. Steel, P. Palese, Influenza virus transmission is dependent on relative humidity and temperature. *PLoS Pathog.* **3**, e151 (2007).
12. K. M. Gustin *et al.*, Environmental conditions affect exhalation of H3N2 seasonal and variant influenza viruses and respiratory droplet transmission in ferrets. *PloS One* **10**, e0125874 (2015).
13. T. A. Jacobson *et al.*, Direct human health risks of increased atmospheric carbon dioxide. *Nat. Sustainability* **2**, 691–701 (2019).
14. R. Zhao, S. Sun, R. Ding, Conditioning strategies of indoor thermal environment in warm climates. *Energy Build.* **36**, 1281–1286 (2004).
15. G. P. Kenny, A. D. Flouris, A. Yagouti, S. R. Notley, Towards establishing evidence-based guidelines on maximum indoor temperatures during hot weather in temperate continental climates. *Temperature* **6**, 11–36 (2019).
16. T. C. Bulfone, M. Malekinejad, G. W. Rutherford, N. Razani, Outdoor transmission of SARS-CoV-2 and Other respiratory viruses: A systematic review. *J. Infect. Dis.* **223**, 550–561 (2021).
17. D. A. Hardy *et al.*, Accurate measurements and simulations of the evaporation and trajectories of individual solution droplets. *J. Phys. Chem. B* **127**, 3416–3430 (2023).
18. A. Davidse, R. N. Zare, Effect of relative humidity in air on the transmission of respiratory viruses. *Mol. Front. J.* **5**, 5–16 (2021).
19. Y. Jamal *et al.*, Identification of thresholds on population density for understanding transmission of COVID-19. *GeoHealth* **6**, e2021GH000449 (2022).
20. M. Moriyama, W. J. Hugentobler, A. Iwasaki, Seasonality of respiratory viral infections. *Annu. Rev. Virol.* **7**, 83–101 (2020).
21. H. Nair *et al.*, Global burden of respiratory infections due to seasonal influenza in young children: A systematic review and meta-analysis. *The Lancet* **378**, 1917–1930 (2011).
22. M. M. Sajadi *et al.*, Temperature, humidity, and latitude analysis to estimate potential spread and seasonality of coronavirus disease 2019 (COVID-19). *JAMA Netw. Open* **3**, e2011834 (2020).
23. L. Zhao, Y. Qi, P. Luzzatto-Fegiz, Y. Cui, Y. Zhu, COVID-19: Effects of environmental conditions on the propagation of respiratory droplets. *Nano Lett.* **20**, 7744–7750 (2020).
24. H. J. Park *et al.*, The effects of indoor temperature and humidity on local transmission of COVID-19 and how it relates to global trends. *PLoS One* **17**, e0271760 (2022).
25. D. H. Morris *et al.*, Mechanistic theory predicts the effects of temperature and humidity on inactivation of SARS-CoV-2 and other enveloped viruses. *Elife* **10**, e65902 (2021).
26. K. Lin, L. C. Marr, Humidity-dependent decay of viruses, but not bacteria, in aerosols and droplets follows disinfection kinetics. *Environ. Sci. Technol.* **54**, 1024–1032 (2019).

27. E. Lofgren, N. H. Fefferman, Y. N. Naumov, J. Gorski, E. N. Naumova, Influenza seasonality: Underlying causes and modeling theories. *J. Virol.* **81**, 5429–5436 (2007).
28. Y. Wu *et al.*, Effects of temperature and humidity on the daily new cases and new deaths of COVID-19 in 166 countries. *Sci. Total Environ.* **729**, 139051 (2020).
29. C. Merow, M. C. Urban, Seasonality and uncertainty in global COVID-19 growth rates. *Proc. Natl. Acad. Sci. U.S.A.* **117**, 27456–27464 (2020).
30. P. Mecenas, R. T. d. R. M. Bastos, A. C. R. Vallinoto, D. Normando, Effects of temperature and humidity on the spread of COVID-19: A systematic review. *PLoS One* **15**, e0238339 (2020).
31. J. Prussin Aaron *et al.*, Survival of the enveloped virus Phi6 in droplets as a function of relative humidity, absolute humidity, and temperature. *Appl. Environ. Microbiol.* **84**, e00551 (2018).
32. J. E. Benbough, Some factors affecting the survival of airborne viruses. *J. Gen. Virol.* **10**, 209–220 (1971).
33. M. Schuit *et al.*, The influence of simulated sunlight on the inactivation of influenza virus in aerosols. *J. Infect. Dis.* **221**, 372–378 (2020).
34. H. P. Oswin *et al.*, Oxidative stress contributes to bacterial airborne loss of viability. *Microbiol. Spectr.* **11**, e03347-22 (2023).
35. A. Haddrell *et al.*, Differences in airborne stability of SARS-CoV-2 variants of concern is impacted by alkalinity of surrogates of respiratory aerosol. *J. R. Soc. Interface* **20**, 20230062 (2023).
36. S. Dhawan, P. Biswas, Aerosol dynamics model for estimating the risk from short-range airborne transmission and inhalation of expiratory droplets of SARS-CoV-2. *Environ. Sci. Technol.* **55**, 8987–8999 (2021).
37. L. C. Marr, J. W. Tang, J. Van Mullekom, S. S. Lakdawala, Mechanistic insights into the effect of humidity on airborne influenza virus survival, transmission and incidence. *J. R. Soc. Interface* **16**, 20180298 (2019).
38. W. G. Lindsley *et al.*, Quantity and size distribution of cough-generated aerosol particles produced by influenza patients during and after illness. *J. Occupat. Environ. Hyg.* **9**, 443–449 (2012).
39. S. Niazi *et al.*, Humidity-dependent survival of an airborne influenza a virus: Practical implications for controlling airborne viruses. *Environ. Sci. Technol. Lett.* **8**, 412–418 (2021).
40. L. Morawska *et al.*, How can airborne transmission of COVID-19 indoors be minimised?. *Environ. Int.* **142**, 105832 (2020).
41. C. Y. H. Chao *et al.*, Characterization of expiration air jets and droplet size distributions immediately at the mouth opening. *J. Aerosol. Sci.* **40**, 122–133 (2009).
42. G. Johnson *et al.*, Modality of human expired aerosol size distributions. *J. Aerosol. Sci.* **42**, 839–851 (2011).
43. M. T. Dulay *et al.*, Effect of relative humidity on hydrogen peroxide production in water droplets. *QRB Discov.* **2**, e8 (2021).
44. M. I. Jacobs, R. D. Davis, R. J. Rapf, K. R. Wilson, Studying chemistry in micro-compartments by separating droplet generation from ionization. *J. Am. Soc. Mass Spectrom.* **30**, 339–343 (2018).
45. A. J. Colussi, Mechanism of hydrogen peroxide formation on sprayed water microdroplets. *J. Am. Chem. Soc.* **145**, 16315–16317 (2023).
46. X. Song, C. Basheer, R. N. Zare, Making ammonia from nitrogen and water microdroplets. *Proc. Natl. Acad. Sci. U.S.A.* **120**, e2301206120 (2023).
47. M. A. Mehrgardi, M. Mofidfar, R. N. Zare, Sprayed water microdroplets are able to generate hydrogen peroxide spontaneously. *J. Am. Chem. Soc.* **144**, 7606–7609 (2022).
48. J. K. Lee *et al.*, Spontaneous generation of hydrogen peroxide from aqueous microdroplets. *Proc. Natl. Acad. Sci. U.S.A.* **116**, 19294–19298 (2019).
49. A. Quinn, J. Shaman, Health symptoms in relation to temperature, humidity, and self-reported perceptions of climate in New York City residential environments. *Int. J. Biometeorol.* **61**, 1209–1220 (2017).
50. S. J. Reynolds *et al.*, Indoor environmental quality in six commercial office buildings in the midwest United States. *Appl. Occupat. Environ. Hyg.* **16**, 1065–1077 (2001).
51. R. R. Netz, Mechanisms of airborne infection via evaporating and sedimenting droplets produced by speaking. *J. Phys. Chem. B* **124**, 7093–7101 (2020).
52. W. Yang, L. C. Marr, Mechanisms by which ambient humidity may affect viruses in aerosols. *Appl. Environ. Microbiol.* **78**, 6781–6788 (2012).
53. Z. Qian *et al.*, Variability in donor lung culture and relative humidity impact the stability of 2009 pandemic H1N1 influenza virus on nonporous surfaces. *Appl. Environ. Microbiol.* **89**, e0063323 (2023).
54. Y. Geng, Y. Wang, Stability and transmissibility of SARS-CoV-2 in the environment. *J. Med. Virol.* **95**, e28103 (2023).
55. A. J. French *et al.*, Environmental stability of enveloped viruses is impacted by initial volume and evaporation kinetics of droplets. *mBio* **14**, e0345222 (2023).
56. C. K. Irwin *et al.*, Using the systematic review methodology to evaluate factors that influence the persistence of influenza virus in environmental matrices. *Appl. Environ. Microbiol.* **77**, 1049–1060 (2011).
57. A. C. Lowen, J. Steel, S. Mubareka, P. Palese, High temperature (30 C) blocks aerosol but not contact transmission of influenza virus. *J. Virol.* **82**, 5650–5652 (2008).
58. J. L. Santarpia *et al.*, Aerosol and surface contamination of SARS-CoV-2 observed in quarantine and isolation care. *Sci. Rep.* **10**, 12732 (2020).
59. K. Lin, C. R. Schulte, L. C. Marr, Survival of MS2 and Φ6 viruses in droplets as a function of relative humidity, pH, and salt, protein, and surfactant concentrations. *PLoS One* **15**, e0243505 (2020).
60. T. Kakeshpour, A. Bax, Simultaneous quantification of H2O2 and organic hydroperoxides by 1H NMR spectroscopy. *Anal. Chem.* **94**, 5729–5733 (2022).